Influence of defect density on the ZnO nanostructures of dye-sensitized solar cells

**Yan-Yan Lou · Shuai Yuan · Yin Zhao ·
Zhu-Yi Wang · Li-Yi Shi**

Abstract The relationship between bilayer nanostructure, defect density and dye-sensitized solar cell (DSCC) performances was investigated. By adjusting bilayer nanostructures, defect density of ZnO nanodendrite-nanorods structure was decreased comparing to that of nanoflower-nanorods structure. The performances of DSCC based on ZnO nanodendrites-nanorods structure and nanoflower-nanorods structure were studied by Raman spectrum, room temperature photoluminescence, dye loading, photocurrent density-voltage characteristic and open-circuit voltage decay (OCVD) technique. The device with nanodendrite-nanorods structure has lower charge recombination rate and prolonged electron lifetime due to its microstructure feature.

Keywords ZnO · Bilayer · Nanostructure · Nanodendrite-nanorods defect · Dye-sensitized solar cells

1 Introduction

Dye sensitized solar cells (DSSCs) have been studied as attractive alternatives for photoelectricity from solar light due to their high efficiency and commercial application prospect. In DSSC, electrons are excited from dyes by light and transferred to nanostructure semiconductor and conducting substrate electrode. However, electrons in semiconductor interface are easily recombined with the holes in electrolyte. The competition between electron transport in semiconductor and electron recombination in semiconductor/dye/electrolyte interface is the key for high performance of DSSCs. There are two strategies usually employed to improve the competition including accelerating electron transport and restraining electron recombination. For the first one, traditional TiO_2 can be replaced with ZnO since it has higher electronic mobility. For the second strategy, reducing surface defects density will decrease the number of trapping electrons on semiconductor surface, hence restraining electron recombination.

Owning to the easy crystallization and anisotropic growth, various ZnO nanostructures such as nanoparticles [1–3], nanorods [4–8], nanotubes [9–12], nanoflowers [13], nanosheets [14], tetrapods [15], nanotrees [16], nanowire-nanosheet [17], nanoforest [18], nanodendrite/nanoparticle composite [19] and multilayer nanowires [20] have been reported in DSSCs. Researchers generally focused on the design of various nanostructured semiconducting materials with emphasis on optimizing dye loading, and less on ZnO material properties themselves such as defect concentration. The defect of ZnO material plays the critical roles in the electron transport and collection in DSSC performance. Recently, annealing [21], optimizing growth process [22], decorating Au nanoparticles [23] or covering ZnS shell [24] have been applied to decrease the defects of ZnO materials. However, the relationships between defect density from the ZnO nanostructures and DSSC performances are still ambiguous.

In this paper, we altered the microstructure of ZnO material to lower defect density on the DSCC performance.

Y.-Y. Lou · S. Yuan (✉) · Y. Zhao · Z.-Y. Wang · L.-Y. Shi (✉)
Research Center of Nanoscience and Nanotechnology, Shanghai University, Shanghai 200444, People's Republic of China
e-mail: s.yuan@shu.edu.cn

L.-Y. Shi
e-mail: shiliyi@shu.edu.cn

Y.-Y. Lou
Laboratory for Microstructures, Shanghai University, Shanghai 200444, People's Republic of China

A bilayer ZnO structure consisting of nanodendrites on top and nanorods at bottom as DSCCs photoanode was compared to that of bilayer nanoflower-nanorods structure. The relationship between bilayer structure, defect density and DSSC performances was investigated by Raman spectrum, room temperature photoluminescence, dye loading, photocurrent density-voltage characteristic and open-circuit voltage decay (OCVD) technique.

2 Experimental

2.1 Fabrication of ZnO hierarchical nanostructure

Firstly, clear ZnO seed solution was obtained by dissolving 0.375 mol/L zinc acetate and ethanolamine in 1:1 molar ratio into 50 mL ethylene glycol monomethyl ether and stirring at 60 °C for 30 min. Then compact ZnO seed layer was formed by dip-coating seed solution onto FTO substrates and heating at 550 °C for 90 min. The nanostructures were fabricated by using hydrothermal method in Teflon-lined autoclaves, where the substrates were immersed slantways into an aqueous solution of 0.12 mol/L zinc nitrate hexahydrate $(Zn(NO_3)_2 \cdot 6H_2O)$, ammonia $(NH_3 \cdot H_2O)$ and 75 mL distilled water. The ammonia concentration was 1.2 mol/L for nanodendrite-nanorod structure and 0.96 mol/L for nanoflower-nanorod structure. The autoclaves were sealed and heated at 90 °C for 4 h, then cooled in air. Then, the solution was refreshed, and the growth was repeated at 90 °C for another 4 h. Finally, the film was taken out of the solution, rinsed with distilled water and dried at room temperature for subsequent characterizations.

2.2 Assembly of DSSCs

FTO substrates with different ZnO nanostructures were immersed in 3 mmol/L N719 dye solution with a mixture solvent of tertiary butanol and acetonitrile(1:1, v/v) for 30 min. The samples were then rinsed with ethanol to remove excessive dye and dried in air at room temperature. For the assembly of solar cells, the photoanodes with 0.25 cm^2 working area were assembled and sealed with 60 µm hot-melt surlyn ring to the counter-electrodes (Pt-coated FTO glass). The iodide-based electrolyte, consisting of 0.1 mol/L LiI, 0.0125 mol/L I$_2$, 0.5 mol/L 4-tert-butylpyridine, and 0.6 mol/L tetrabutylammonium iodide in acetonitrile, was injected into the interelectrode space from the counter-electrode side through a predrilled hole.

2.3 Characterizations

The morphologies of different ZnO nanostructures were observed using a JEOL JSM-6700F scanning electron microscope (SEM). The X-ray diffractometer (XRD) analysis for the crystal structure was carried out in a Rigaku D/max 2500 v+/pc diffractometer with Cu Ka radiation ($\lambda = 1.5405$ nm). Raman spectrum was measured by Renishaw INVIA Raman spectrometer with 532 nm laser light (Nd:YAG) laser as an excitation source. The dye absorption amount was determined by desorbing dye molecules in 0.1 mol/L NaOH solution of water and ethanol (50:50, v/v) [25] and the dyes absorption spectrum was measured by a UV–vis spectrophotometer (Shimadzu UV-2501 PC). The photoluminescence spectrum measurement was excited by 330 nm laser at room temperature by Horiba HR800 UV. Photocurrent density-voltage (J-V) curves were recorded using Keithley 2400 digital source meter. The light source is 500 W Xenon lamp (San-Ei Electric, XES-151S) and calibrated to 100 mW/cm^2 with standard Si solar cell. The OCVD characteristics were conducted by monitoring the subsequent decay of V_{oc} after shutting down the illumination on DSSC under open-circuit conditions.

3 Results and discussion

3.1 ZnO film with different nanostructures

The bilayer nanoflower-nanorod structure consists of nanoflower layer on top and nanorod array at bottom (see Figs. 1a, b, e), while the nanodendrite-nanorod structure (see Figs. 1c, d, f) has nanodendrite layer on top and nanorod array at bottom. The randomly distributed nanoflowers or nanodendrites are of 10 µm size and connected tightly to the bottom layer. Similar thickness in both structures is achieved. The nanoflower (see Fig. 1e) or nanodendrite layer (see Fig. 1f) is estimated about 8 µm in thickness. The thickness of nanorod array layer of both structures are about 6 µm. Individual flower-shaped nanostructure on top layer of nanoflower-nanorod structure is composed of many hexagonal plane-tipped nanorods with 200-300 nm diameter and 5 µm length. These nanorods originate from one center and grow outwards, exhibiting a chrysanthemum flower shape. While nanodendrite-nanorod structure shows nanodendrite shape on top layer, but quite similar to flower shape. A close look at the nanodendrite structure reveals that the branches are needle-like nanorods with 100 nm diameter and 800 nm in length. The backbones are almost twice larger diameter (400–500 nm) but similar (5–6 µm length) compared to the petal of nanoflower-nanorod structure.

The difference of morphology between nanoflower-nanorod and nanodendrite-nanorod structure is due to the different ammonia contents in the initial reaction solution. The excessive ammonia in the reaction solution on the
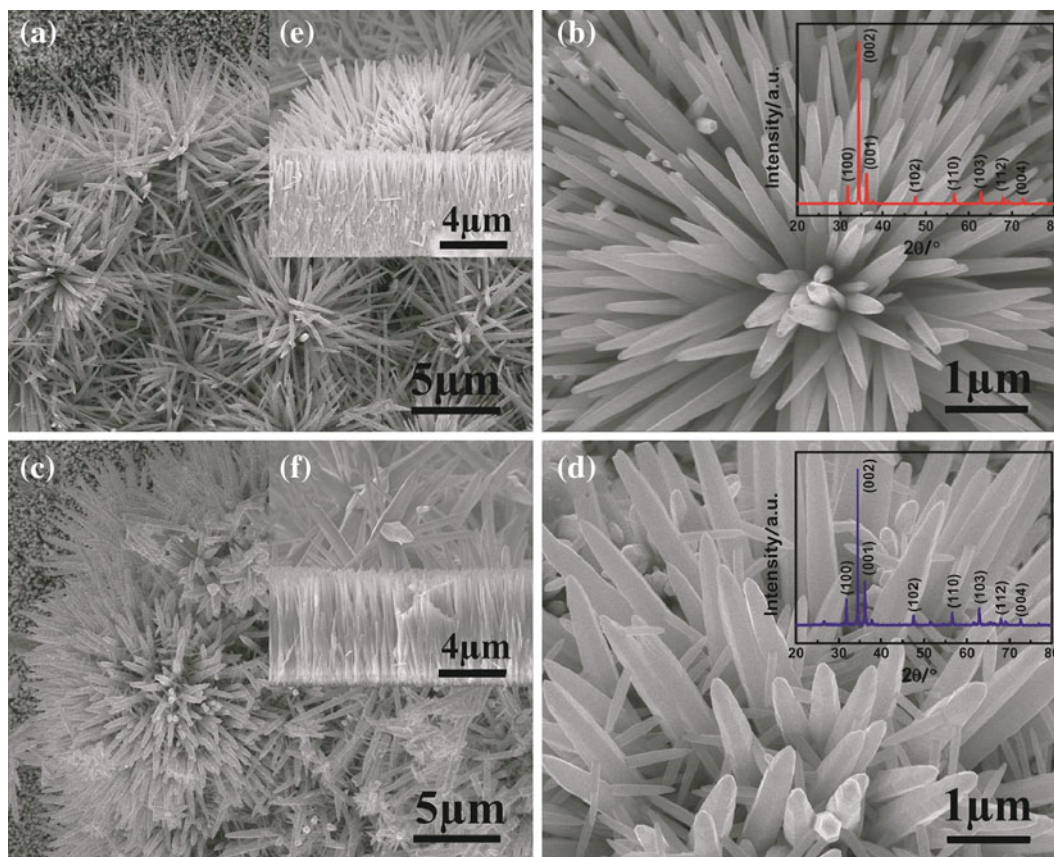
Fig. 1 (**a**) *Top-view*, (**b**) high-magnification and (**e**) *side-view* SEM images of nanoflower-nanorod structure; (**c**) the top-view, (**d**) high-magnification and (**f**) *side-view* SEM images of nanodendrite-nanorod structure. The *inset curves* in (**b**) and (**d**) are the XRD patterns of nanoflower-nanorod structure and nanodendrite-nanorod structure

second growth circle leads to the slight melting of the surface on the backbones of nanodendrite [26, 27]. The renucleation and sequential growth of nanorods happens on the surface defects of backbones by further reducing their energy through the surface reconstruction [28], resulting in the formation of the complex three-dimensional ZnO nanodendrite-nanorod structure.

XRD patterns of nanoflower-nanorod and nanodendrite-nanorod structures (see insert of Figs. 1b, d) are all indexed as hexagonal wurtzite structure according to JCPDS card No.36-1451). No excess peaks are detected, implying the high-purity of both ZnO nanostructures synthesized by the hydrothermal method. The obtained XRD patterns are dominated by (002) peak, which is in agreement with the structure of *c*-axis oriented bottom layer and multi-oriented top layer. The relative peak ratios of (002)/(100) and (002)/(101) of both structures are listed in Table 1. The less (002) orientation of nanodendrite-nanorod structure indicates its more lateral growth contrasting to the nanoflower-nanorod one.

Raman-scattering spectra of nanodendrite-nanorod and nanoflower-nanorod structures normalized by the highest peak are employed to analyze their crystal structures and

Table 1 Relative peak ratios of nanoflower-nanorod and nanodendrite-nanorod structures in XRD patterns

Sample	(002)/(100)	(002)/(101)
Nanoflower-nanorod structure	8.5	5.5
Nanodendrite-nanorod structure	6.4	3.2

defects (see Fig. 2a). The crystal structure of ZnO is wurtzite (hexagona) and belongs to the C_{6v}^4 space group. It has two formula units per primitive cell, and all atoms occupy the C_{3v} sites. According to the Group theory, there are eight sets of zone centre optical phonons, where A_1 and E_1 modes are polarized and split into transverse optical (A_{1T} and E_{1T}) and longitudinal optical (A_{1L} and E_{1L}) phonons, while the E_2 mode consists of two Raman-active modes: low- and high-frequency phonons (E_{2L} and E_{2H}). The dominated peak at 437 cm^{-1}, labeled as E_2, is the characteristic of ZnO wurtzite hexagonal phase (see Fig. 2a). Peak at 330 cm^{-1} is the second-order Raman spectrum, originating from the zone boundary phonons $3E_{2H}$–E_{2L}. And peak at 380 cm^{-1} can be labeled as A_{1T}. The peak at 580 cm^{-1} assigned to E_{1L} is also observed.
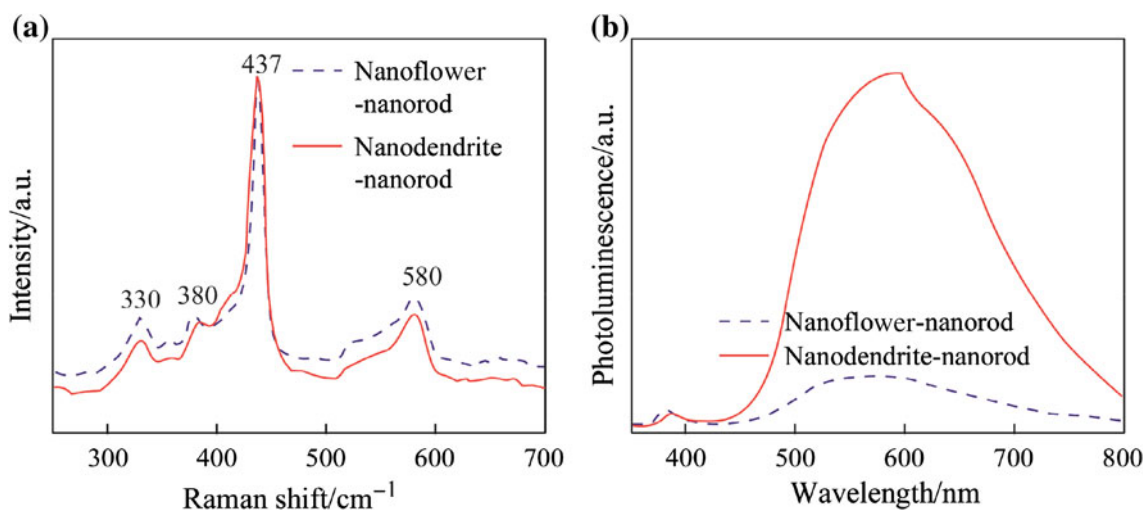
Fig. 2 (**a**) Raman spectra and (**b**) the photoluminescence spectra

Generally, it is related to the formation of defects in ZnO (oxygen vacancies and Zn interstitials) [29]. The lower E_{1L} signal in nanodendrite-nanorod structure indicates the fewer defects in ZnO crystal structure.

Room temperature photoluminescence is also used to study ZnO intrinsic defects in both structures (see Fig. 2b). UV emission around 380 nm is near band edge emission resulting from the recombination of free excitons. Green emission centered at 500-600 nm is the surface-state related defect emission, originating from the recombination of singly ionized oxygen vacancy with holes in the valence band. Nanodendrite-nanorod structure has much lower green emission and relatively higher UV emission than the nanoflower-nanorod one. The results indicate the nanodendrite-nanorod structure possesses better optical property and fewer defects comparing to nanoflower-nanorod one.

3.2 Performance of DSSCs

The photocurrent density-voltage characteristics of DSSCs based on nanoflower-nanorod and nanodendrite-nanorod structured ZnO are obtained at AM 1.5 irradiation of 100 mW/cm^2 (see Fig. 3). The detailed photovoltaic performance parameters of DSSCs with different structures are listed in Table 2. The short-circuit photocurrent density (J_{sc}), open-circuit voltage (V_{oc}) and fill factor (F_f) of device with nanoflower-nanorod structured ZnO are 5.07 mA/cm^2, 545.98 mV and 0.37, respectively, leading to 1.01% of energy conversion efficiency. While the performances of the DSSC with nanodendrite-nanorod structure are improved by 20%, 3% and 8% in J_{sc}, V_{oc} and F_f, respectively, finally resulting in 35% increase in energy conversion efficiency.

The short-circuit current of DSSC is mainly influenced by the light harvesting and charge recombination at
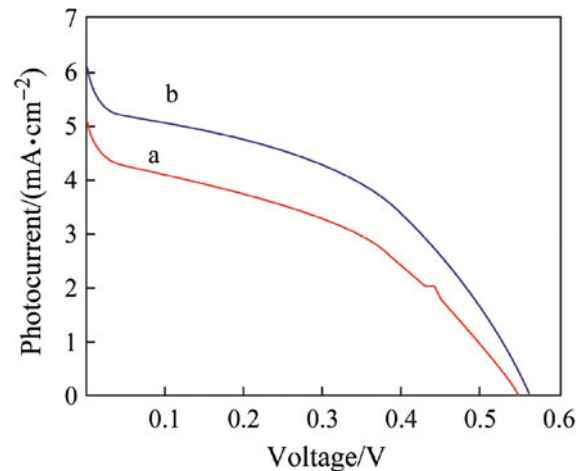

Fig. 3 J–V curves of DSSCs nanoflower-nanorod a and nanodendrite-nanorod structures b

Table 2 Performances of DSSCs with nanoflower-nanorod and nanodendrite-nanorod structured ZnO

Sample	$J_{sc}/$ (mA·cm^{-2})	V_{oc} / mV	FF	η / %
Nanoflower-nanorod structure	5.07	545.98	0.37	1.01
Nanodendrite-nanorod structure	6.09	561.33	0.40	1.36

photoanode [30–32]. Based on the approximate thickness of films (see Figs. 1e, f), the similar dye absorption of different structures is achieved (see Fig. 4). The absorption of dye adsorbed on nanodendrite-nanorod and nanoflower-nanorod structured ZnO is almost of the same value at 380 nm and 521 nm, which is the maximum absorption peak of N719 dye. The values of dye adsorption on the
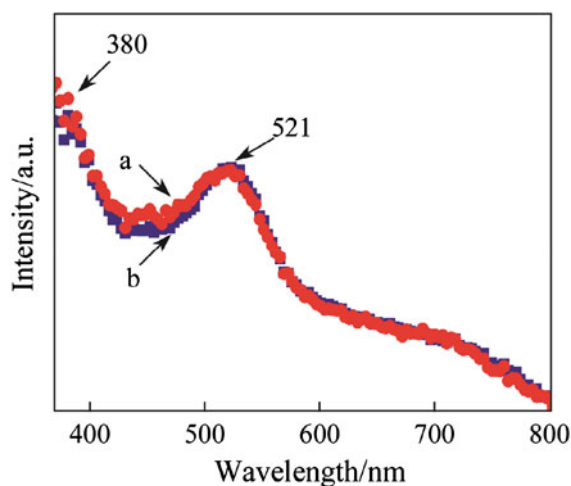
Fig. 4 UV–vis absorption spectra for dyes desorbed from nanoflower-nanorod *a* and nanodendrite-nanorod structured ZnO *b*

nanodendrite-nanorod and nanoflower-nanorod structured ZnO are 3.2×10^{-7} mol/cm^2 and 3.1×10^{-7} mol/cm^2, respectively. Compared with the nanoflower-nanorod structure, the increased surface area in nanodendrite-nanorod structure by the formation of needle-like branch is offset by the large diameter/length ratio of the petals on the top layer. It suggests that the dye loading amount is not responsible for the increased J_{sc} in the DSSC with nanodendrite-nanorod structured ZnO. Therefore, a lower charge recombination rate of nanodendrite-nanorod structures may be the main reason for the enhanced DSSC performance. It is believed that the decreased carrier recombination at the dye/ZnO interface can be obtained by lower concentration of surface defects in ZnO material [33]. Hence, fewer defects in nanodendrite-nanorod

nanostructure as demonstrated by Raman and photoluminescence analysis, may lead to improved device performance.

The OCVD technique as a powerful tool to study the electron lifetime in DSSC can provide some quantitative information on the electron recombination in DSSC [34]. By recording the subsequent decay of photovoltage (V_{oc}) after turning off the illumination in the steady state, the recombination rate of photoelectrons is monitored. In other words, the recombination rate of photoelectrons is proportional to the rate of photovoltage decay [32]. The OCVD response of the DSSC with nanodendrite-nanorod structure is much slower than the one with nanoflower-nanorod structure (see Fig. 5a).

From the OCVD experiment, the electron lifetime (τ) is determined by the reciprocal of the derivative of the decay curves normalized by the thermal voltage [34], using the following equation:

$$\tau = -\frac{k_B T}{e}\left(\frac{dV_{OC}}{dt}\right)^{-1}, \tag{1}$$

where k_B the Boltzmann constant, T the absolute temperature, e the elementary positive charge, and dV_{oc}/dt the derivative of the transient open-circuit voltage.

The results of electron lifetime on the open-circuit voltage of DSSCs with different structures clearly demonstrate that, at any given open circuit potential, the electron lifetime of DSSC with nanodendrite-nanorod structure is longer than that of nanoflower-nanorod one (see Fig. 5b). The prolonged electron lifetime should be attributed to the lower electron recombination caused by the fewer defects in the nanodendrite-nanorod structure. The more efficient electron transport channel finally leads to higher energy conversion efficiency.
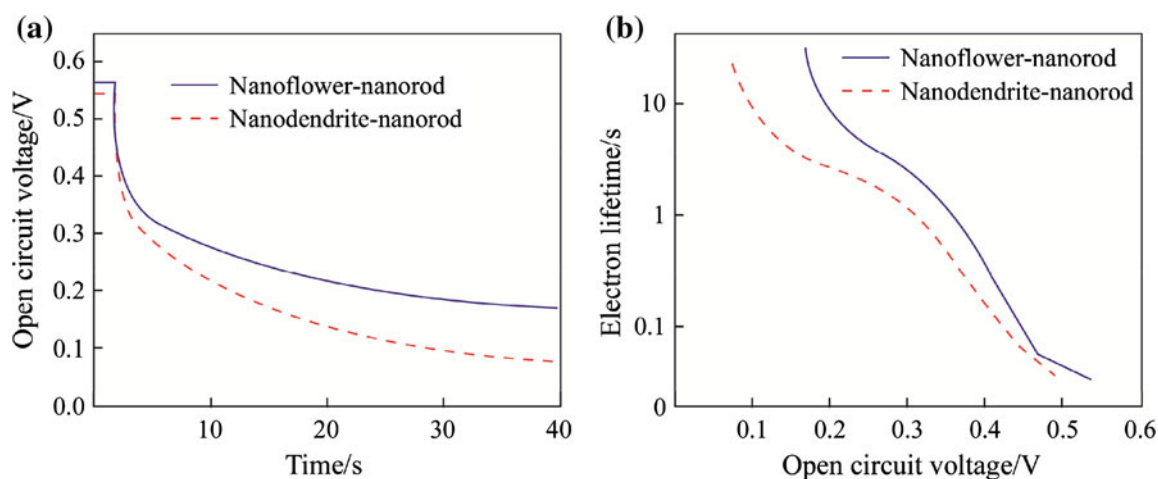

Fig. 5 (**a**) OCVD curves and (**b**) the comparison of electron lifetime (in log-linear representation) as a function of open-circuit voltage of DSSCs

4 Conclusions

In summary, by tuning the microstructures, defect density of ZnO bilayer nanodendrite-nanorod structure was decreased comparing to that of nanoflowers-nanorods structure. The performance of DSSC with nanodendrite-nanorod structure has lower charge recombination rate, prolonged electron lifetime and enhanced photocurrent due to its microstructure feature.

References

1. Lu X, Huang F, Mou X, Wang Y, Xu F (2010) A general preparation strategy for hybrid TiO_2 hierarchical spheres and their enhanced solar energy utilization efficiency. Adv Mater 22:3719–3722
2. Liu Z, Liu C, Ya J (2010) Preparation of ZnO nanoparticles and characteristics of dye-sensitized solar cells based on nanoparticles film. Solid State Sci 12:111–114
3. Wong KK, Ng A, Chen XY et al (2012) Effect of ZnO nanoparticle properties on dye-sensitized solar cell performance. ACS Appl Mater Interfaces 4:1254
4. Zhang Y, Chen J, Li C et al (2011) Incorporation of graphene in quantum dot sensitized solar cells based on ZnO nanorods. Chem Commun 47:6084–6086
5. Yengantiwar A, Sharma R, Game O, Banpurkar A (2011) Growth of aligned ZnO nanorods array on ITO for dye sensitized solar cell. Curr Appl Phys 11:S113–S116
6. Lee Y-M, Yang H-W (2011) Optimization of processing parameters on the controlled growth of ZnO nanorod arrays for the performance improvement of solid-state dye-sensitized solar cells. J Solid State Chem 184:615–623
7. Chen J, Lei W, Li C et al (2011) Flexible quantum dot sensitized solar cell by electrophoretic deposition of CdSe quantum dots on ZnO nanorods. Phys Chem Chem Phys 13:13182–13184
8. Chung J, Lee J, Lim S (2010) Annealing effects of ZnO nanorods on dye-sensitized solar cell efficiency. Phys B 405:2593–2598
9. Han J, Fan F, Xu C et al (2010) ZnO nanotube-based dye-sensitized solar cell and its application in self-powered devices. Nanotechnology 21:405203
10. Ameen S, Akhtar MS, Kim YS, Yang OB, Shin HS (2011) Influence of seed layer treatment on low temperature grown ZnO nanotubes: performances in dye sensitized solar cells. Electrochim Acta 56:1111–1116
11. Martinson AB, Elam JW, Hupp JT, Pellin MJ (2007) ZnO nanotube based dye-sensitized solar cells. Nano Lett 7:2183–2187
12. Liu Z, Liu C, Ya J, Lei E (2011) Controlled synthesis of ZnO and TiO_2 nanotubes by chemical method and their application in dye-sensitized solar cells. Renew Energy 36:1177–1181
13. Jiang CY, Sun XW, Lo GQ, Kwong DL, Wang JX (2007) Improved dye-sensitized solar cells with a ZnO-nanoflower photoanode. Appl Phys Lett 90:263501
14. Akhtar MS, Hyung JH, Yang OB, Cho NK, Hwang HI, Lee SK (2010) Thermally grown ZnO nanosheets for high efficiency dye-sensitized solar cells. J Nanosci Nanotechnol 10:3654
15. Chen W, Yang S (2011) Dye-sensitized solar cells based on ZnO nanotetrapods. Frontiers Optoelectron China 4:24–44
16. Qiu J, Guo M, Feng Y, Wang X (2011) Electrochemical deposition of branched hierarchical ZnO nanowire arrays and its photoelectrochemical properties. Electrochim Acta 56:5776–5782
17. Xu F, Dai M, Lu Y, Sun L (2010) Hierarchical ZnO nanowire-nanosheet architectures for high power conversion efficiency in dye-sensitized solar cells. J Phys Chem C 114:2776–2782
18. Ko SH, Lee D, Kang HW et al (2011) Nanoforest of hydrothermally grown hierarchical ZnO nanowires for a high efficiency dye-sensitized solar cell. Nano Lett 11:666–671
19. Wu CT, Liao WP, Wu JJ (2011) Three-dimensional ZnO nanodendrite/nanoparticle composite solar cells. J Mater Chem 21:2871–2876
20. Gao D, Xu CK, Wu JM, Desai UV (2011) Multilayer assembly of nanowire arrays for dye-sensitized solar cells. J Am Chem Soc 133:8122–8125
21. Kyaw HH, Bora T, Dutta J (2012) One-diode model equivalent circuit analysis for ZnO nanorod-based dye-sensitized solar cells: effects of annealing and active area. IEEE Trans Nanotechnol 11:763–768
22. Jung J, Myoung J, Lim S (2012) Effects of ZnO nanowire synthesis parameters on the photovoltaic performance of dye-sensitized solar cells. Thin Solid Films 520:5779–5789
23. Sarkar S, Makhal A, Bora T, Baruah S, Dutta J, Pal SK (2011) Photoselective excited state dynamics in ZnO–Au nanocomposites and their implications in photocatalysis and dye-sensitized solar cells. Phys Chem Chem Phys 13:12488
24. Chung J, Myoung J, Oh J, Lim S (2010) Synthesis of a ZnS shell on the ZnO nanowire and its effect on the nanowire-based dye-sensitized solar cells. J Phys Chem C 114:21360–21365
25. Wu MK, Ling T, Xie Y, Huang XG, Du XW (2011) Performance comparison of dye-sensitized solar cells with different ZnO photoanodes. Semicond Sci Technol 26:105001
26. Sounart TL, Liu J, Voigt JA, Huo M, Spoerke ED, McKenzie B (2007) Secondary nucleation and growth of ZnO. J Am Chem Soc 129:15786–15793
27. Xu L, Chen Q, Xu D (2007) Hierarchical ZnO nanostructures obtained by electrodeposition. J Phys Chem C 111:11560–11565
28. Gao Y, Koumoto K (2005) Bioinspired ceramic thin film processing: present status and future perspectives. Cryst Growth Des 5:1983–2017
29. Vanheusden K, Warren WL, Seager CH, Tallant DR, Voigt JA, Gnade BE (1996) Mechanisms behind green photoluminescence in ZnO phosphor powders. J Appl Phys 79:7983
30. O'Regan BC, Durrant JR, Sommeling PM, Bakker NJ (2007) Influence of the $TiCl_4$ treatment on nanocrystalline TiO_2 films in dye-sensitized solar cells. 2. Charge density, band edge shifts, and quantification of recombination losses at short circuit. J Phys Chem C 111:14001–14010
31. Green ANM, Palomares E, Haque SA, Kroon JM, Durrant JR (2005) Charge transport versus recombination in dye-sensitized solar cells employing nanocrystalline TiO_2 and SnO_2 films. J Phys Chem B 109:12525
32. Yu H, Zhang S, Zhao H, Will G, Liu P (2009) An efficient and low-cost TiO_2 compact layer for performance improvement of dye-sensitized solar cells. Electrochim Acta 54:1319–1324
33. Quintana M, Edvinsson T, Hagfeldt A, Boschloo G (2007) Comparison of dye-sensitized ZnO and TiO_2 solar cells: studies of charge transport and carrier lifetime. J Phys Chem C 111:1035–1041
34. Zaban A, Greenshtein M, Bisquert J (2003) Determination of the electron lifetime in nanocrystalline dye solar cells by open-circuit voltage decay measurements. ChemPhysChem 4:859–864